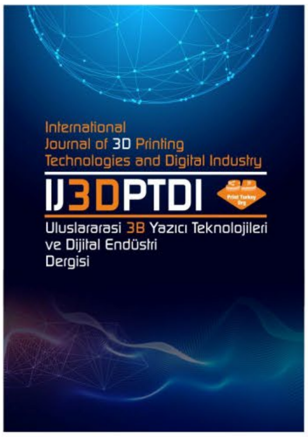

ULUSLARARASI 3B YAZICI TEKNOLOJİLERİ
VE DİJİTAL ENDÜSTRİ DERGİSİ

INTERNATIONAL JOURNAL OF 3D PRINTING TECHNOLOGIES AND DIGITAL INDUSTRY

ISSN:2602-3350 (Online)

URL: https://dergipark.org.tr/ij3dptdi

COMPARATIVE ANALYSIS OF BCCZZ LATTICE STRUCTURE COMPRESSION BEHAVIOR: EXPERIMENTAL, NUMERICAL, AND MACHINE LEARNING APPROACHES

Yazarlar (Authors): Deniz Aktürk *, Muhammed Taha Yildiz, Nazim Babacan

Bu makaleye şu şekilde atıfta bulunabilirsiniz (To cite to this article): *Aktürk D., Yildiz M. T., Babacan N., "Comparative Analysis of BCCZZ Lattice Structure Compression Behavior: Experimental, Numerical, and Machine Learning Approaches" Int. J. of 3D Printing Tech. Dig. Ind., 9(1): 36-44, (2025).*

DOI: 10.46519/ij3dptdi.1490522

Araştırma Makale/ Research Article

Erişim Linki: (To link to this article): https://dergipark.org.tr/en/pub/ij3dptdi/archive

COMPARATIVE ANALYSIS OF BCCZZ LATTICE STRUCTURE COMPRESSION BEHAVIOR: EXPERIMENTAL, NUMERICAL, AND MACHINE LEARNING APPROACHES

Deniz Aktürk [a, b, *], Muhammed Taha Yildiz [a, b], Nazim Babacan [a]

[a] Department of Mechanical Engineering, Sivas University of Science and Technology, TÜRKİYE
[b] Institute of Defence Technologies, Sivas University of Science and Technology, TÜRKİYE

[*] *Corresponding Author: dakturk@sivas.edu.tr*

(**Received:** 27.05.24; **Revised:** 07.10.24; **Accepted:** 12.02.25)

ABSTRACT

In this study, the compression behavior of the body-centered cubic with exterior and interior vertical struts (BCCZZ) lattice structure produced with Polylactic Acid (PLA) has been investigated using experimental, numerical, and machine-learning algorithms. When comparing digital image correlation and the ANSYS Static Structural numerical module, the measurements of deformation in the -Y direction taken from the top-right, top-left, middle-right, and middle-left points of the lattice structure are closely matched, with differences of 3.5%, 0.66%, 22.3%, and 12.69%, respectively. However, measurements from the bottom-left and bottom-right points show discrepancies of 49.17% and 58.91%, respectively. The lack of agreement between numerical and digital image correlation (DIC) analyses at the bottom-left and bottom-right points of the lattice structure is attributed to deformation in the lower section observed in the experimental study. The numerical study, modeling only elastic deformation, fails to account for broken regions' deformation adequately. Furthermore, the elastic deformation region has been comparatively investigated using experimental, numerical, and multilinear regression (MLR) models. Despite the MLR algorithm being trained with data from the compression test and achieving an R^2 value of 0.97, numerical modeling is closer to the experimental results. Thus, for the first time in the literature, the compression behavior of the BCCZZ lattice structure made from PLA+ has been comparatively investigated using experimental, numerical, and machine learning methods.

Keywords: Additive Manufacturing, Lattice Structure, Digital Image Correlation, Numerical Modeling, Machine Learning, Compression Behavior.

1.INTRODUCTION

In recent years, the popularity of additive manufacturing methods has increased due to rapid prototyping, allowing the production of materials with desired tolerance and complexity [1, 2]. This manufacturing technique was first implemented in 1986 through the stereolithography technique, and over years of development, it has continued to evolve with techniques such as selective laser melting and fused deposition modeling (FDM) [3-5]. These methods are utilized in numerous sectors, including the aerospace, automotive, medical implants, and the defense industry [6-9].

FDM technology has emerged as the foremost additive manufacturing method for producing polymeric components, owing to its ease of implementation and cost-effectiveness [10]. In terms of polymer materials, polylactic acid (PLA) and acrylonitrile butadiene styrene (ABS) are the most commonly utilized, facilitating additive manufacturing in practical applications [11]. These thermoplastics, prized for their lightweight nature and affordability, are extensively favored in engineering and medical sectors [12]. PLA has earned its popularity in various applications due to its exceptional qualities, including biocompatibility, biodegradability, mechanical strength, and processability [13].

In many engineering applications, lattice structures, which can be manufactured by additive manufacturing methods such as FDM technology, have become increasingly important due to their energy absorption capabilities and lightweight properties [14, 15]. Lattice structures are configurations created by connecting struts with three-dimensional geometry to nodes in a repeating cell pattern [16]. These structures are referred to by different names based on their arrangements, with the most commonly used being body-centered cubic (BCC) and face-centered cubic (FCC) structures [17]. These structures are referred to as BCCZ and FCCZ with the addition of vertical z-struts. The inclusion of these z-struts enhances the resistance to yielding and deformation in both BCC and FCC configurations [18-21]. Zhou et al. [22] have numerically and experimentally investigated the compression behavior of four different lattice geometries produced with PLA. They found that BCCZ and FCCZ lattice structures have a higher load-bearing capacity compared to BCC structures. In a recent study [23], the novel BCCZZ structure, featuring extra z-struts situated at the mid-span of oblique struts, was examined. It was found that the additional vertical struts in the BCCZ structures offer greater advantages for load-bearing applications, as they result in higher relative density and relative strength compared to the reference BCCZ structure.

To understand the behavior of lattice structures in load-bearing applications, experimental, analytical, and numerical methods are available [24, 25]. An ideal technique for measuring strain and revealing the deformation and failure mechanisms in lattice structures is a non-contact strain measurement method such as digital image correlation (DIC) [26, 27]. In addition, further insights into the deformation behavior and local strain values of lattice structures can be gained by the finite element method [28]. Moreover, machine learning algorithms, such as multiple linear regression (MLR) algorithm, can predict the behavior of the material under compression based on the features obtained from the compression test data. Once this algorithm developed and validated, the model can be applied to predict the stress-strain data of the similar materials or structures.

Previous studies investigating compression behavior in lattice structures have typically relied on individual approaches like experiments, numerical simulations, or analytical methods, or a combination of two of these methods [27, 29-34]. This study uniquely addresses this gap by comparatively analyzing the compression behavior of a novel BCCZZ lattice structure through using a combined approach of digital image correlation (DIC), numerical method, and machine learning algorithm. Overall, the novelty of the study lies in the integration of multiple approaches to achieve a comprehensive understanding of a lattice structure's compressive behavior and deformation mechanism. It is believed that this integration enhances prediction accuracy, aids in design optimization, and improves the efficiency of engineering analysis processes.

2.MATERIAL AND METHODS

2.1. Experimental Analysis

The productions were performed with an FDM 3D printer (Ender-3 S1-Pro, Creality) at a nozzle temperature of 205 °C and a bed temperature of 65 °C. The lattice structure was made from polylactic acid (PLA+, eSUN) polymer. The dimensions of the produced lattice specimen were designed to be 62.5 x 62.5 x 60 mm^3 with strut diameters of 2.5 mm using the SolidWorks program. The drawing of the model is shown in Figure 1. It was then sliced in the Creality Slicer CAM program and converted into a G-code file for printing with a 10% infill density.

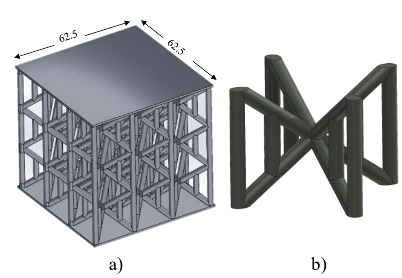

Figure 1. a) The model of the BCCZZ lattice structure and b) A view of the unit BCCZZ cell.

The compression test was conducted using a Shimadzu AG-S 50 kN universal testing machine at a 1 mm/min deformation rate. Three specimens of the BCCZZ lattice structure have been produced, and compression tests have been conducted for each sample. A DIC system (EduDIC, Dantec) was used during the compression test to monitor the strain values in real-time and allow for later comparison with numerical analysis. The sample was sprayed with black speckles in a stochastic pattern. The images were captured at 100 Hz with the DIC system, and experimental data was examined through deformation of 2.5 mm. Figure 2 presents the compression test setup with DIC system. Datasets for numerical and machine learning algorithm analyses were generated from the compression test data.

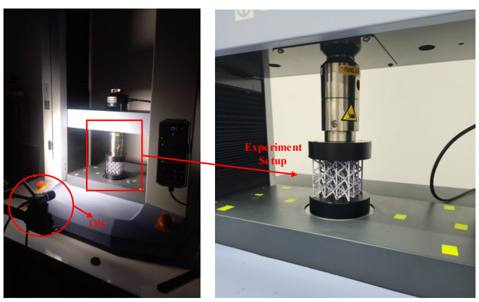

Figure 2. Compression Test Setup with DIC.

2.2. Numerical Analysis

In this study, the compression test of the BCCZZ lattice structure, produced with eSUN: PLA+ material, was numerically modeled. The ANSYS Static Structural module, which utilizes the finite element method for computation, has been used for numerical modeling.

To model the lattice structure produced with eSUN: PLA+, the material parameters shown in Table 1, was used.

Table 1. eSUN: PLA+ Ansys Engineering Data Parameters [35].

Parameters	Value
Density	1.23 g/cm^3
Thermal Expansion Coefficient	0.00135 1/°C
Young Modulus	2.3 GPa
Poisson Ratio	0.3
Bulk Modulus	1.91 GPa
Shear Modulus	8.84 GPa

After conducting a mesh dependency study for element sizes of 0.75, 1, and 1.25 mm, a tetrahedral mesh structure with an element size chosen as 1 mm was utilized for the lattice structure. Figure 3 depicts the details and visual representation of the mesh structure.

a)

b)

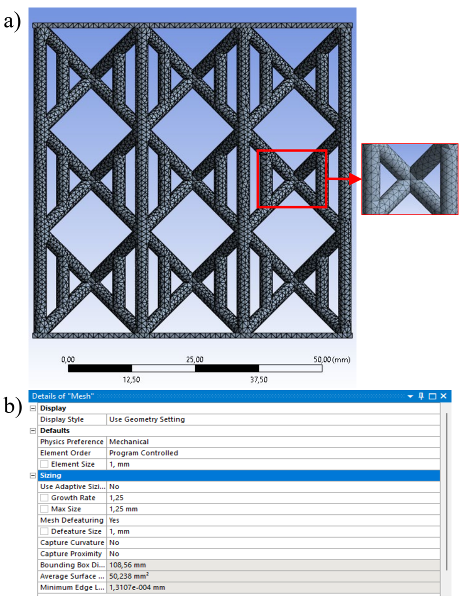

Figure 3. a) BCCZZ Mesh structure and b) Detail of the Mesh.

The compression analysis employed specific boundary conditions: a fixed support at the material's base and a displacement in the -Y direction at the top, set to 2.5 mm. The analysis involved measuring total deformation, total stress, force reaction, and directional deformation at six specific points. These points, depicted in Figure 4, had their directional deformation values measured across compression levels of 0.5, 1, 1.5, 2, and 2.5 mm.

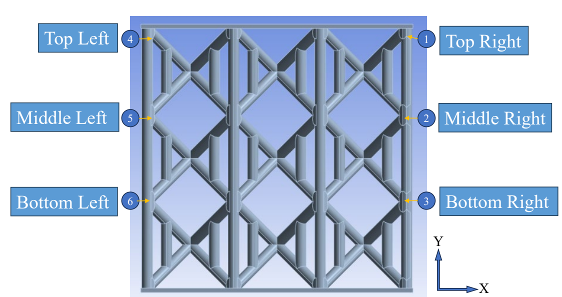

Figure 4. Deformation measurement points at the front face.

2.3. Multilinear Regression Algorithm

Multiple linear regression (MLR), a traditional prediction method, is an algorithm that attempts to predict a target variable based on one input variable [36, 37]. The MLR method possesses a simple, efficient, and data noise-resistant algorithm for predicting data with a linear distribution [38]. The MLR algorithm is shown in Equation (1). "Y " and "x_i" represent the response and predictor variables, respectively, "b_i" and "$\mathcal{E}$" denote the regression and residual coefficients, respectively, and "a" indicates the intercept [39].

$$Y = a + \sum_{i=1}^{n} b_i x_i + \mathcal{E} = b_1 x_1 + b_2 x_2 + \cdots + b_i x_i + \mathcal{E} \qquad (1)$$

The necessary data for MLR were obtained from the elastic deformation region of compression test results. A test size of 0.2 was determined, and the data were trained. In the MLR method, Scikit-learn, Pandas, Matplotlib, Seaborn, and NumPy libraries were used. Analyses were performed using Python 3.11 programming language, with Spyder 5.4.3 IDE. The results obtained with MLR have been comparatively examined with experimental data.

3.RESULTS AND DISCUSSIONS

In this study, the deformation of the BCCZZ lattice structure under compressive loading was investigated using experimental, numerical, and machine learning methods. The DIC results obtained from the experimental analysis were compared with numerical analyses. Furthermore, a machine learning algorithm was trained using the results obtained from the experimental data, and the experimental, numerical, and machine learning results were comparatively analyzed.

Figure 5 displays the total deformation contour images obtained from numerical and DIC analysis results. These images depict various deformation values ranging from 0.5 to 2.5 mm, with intervals of 0.5 mm. Table 2 presents the deformation values in the (-Y) direction at the relevant points (indicated in Figure 4) obtained from numerical test and experimental DIC analysis, as well as their relative differences. Throughout all deformation steps in numerical analyses, the base is experienced minimum deformation, due to the fixed deformation. However, in all deformation steps analyzed using DIC, deformation was observed on the ground. This discrepancy arises because, in the numerical analysis, defining the part as fixed to the ground prevents any deformation on the surface of the part or the ground. In contrast, experimental analyses conducted with DIC have shown deformation on the ground. At 0.5 and 1 mm, neither numerical nor DIC analyses show significant bending in struts. In addition, the BCCZZ lattice structure undergoes transverse expansion and longitudinal shortening while absorbing the force.

In the numerical analyses (Figure 5(e)), the maximum deformation is observed in the bent struts labeled as 1 and 3. Conversely, in the DIC tests (Figure 5(f)), maximum deformation primarily concentrates at the upper regions of the lattice structure, with heightened deformation observed at points where strut bending commences. Similar deformation patterns are noted in the struts within designated regions under deformation points of 1.5, 2, and 2.5 mm, as observed in both numerical and DIC analyses. Furthermore, it is seen that there is no significant shape change in the struts in the central region of the lattice structure in both analyses. This occurs because the presence of neighboring struts in the central region allows the load to be distributed more evenly to the struts at the center point. Thus, it has been observed that contour graphs are highly consistent throughout all deformation steps.

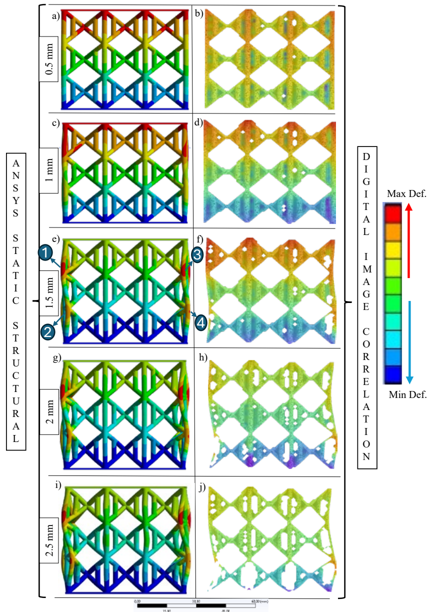

Figure 5. Contour images of the total deformation values from Ansys Static Structural (on the left) and DIC results (on the right).

Table 2 presents the deformation measurements at the points indicated in Figure 4 through numerical and DIC analyses, showing both deformation values and the percentage of absolute relative difference. Meanwhile, Table 3 presents the average percentages of absolute relative differences (ARD) separately. From these findings, it is apparent that the values at the top right, top left, middle right, and middle left points are relatively close to each other, with respective percentages of 3.5%, 0.66%, 22.3%, and 12.69%. However, a discrepancy is observed between the values at the bottom right and bottom left points, which are 58.91% and 49.17%, respectively. This can be attributed to the fact that in numerical analyses, the ground is fixed with fixed support, meaning the lattice structure does not undergo any movement on the surface, while in DIC analyses, the deformation caused by the force applied by the compression device also results in significant deformation of the ground. Additionally, due to fractures occurring in the struts during DIC analysis, the mesh structure that the analysis can track (randomly painted surface) is disrupted, resulting in the inability to capture the deformation at the bottom left, as seen in Figure 5(j).

Table 2. Deformation and ARD (%) values for Ansys Static Structural and DIC

Deformation	Measured Point	Ansys Static Structural	DIC	Absolute Relative Difference (%)
0.5 mm	Top Right	0.485	0.492	1.42
	Middle Right	0.337	0.471	28.45
	Bottom Right	0.172	0.439	60.82
	Top Left	0.485	0.489	0.81
	Middle Left	0.335	0.458	26.85
	Bottom Left	0.172	0.428	59.81
1 mm	Top Right	0.951	0.989	3.84
	Middle Right	0.657	0.838	21.59
	Bottom Right	0.324	0.660	50.90
	Top Left	0.982	0.976	0.61
	Middle Left	0.684	0.815	16.07
	Bottom Left	0.344	0.650	47.07
1.5 mm	Top Right	1.417	1.471	3.67
	Middle Right	1.006	1.228	18.07
	Bottom Right	0.403	0.890	54.71
	Top Left	1.532	1.510	1.45
	Middle Left	1.136	1.157	1.81
	Bottom Left	0.488	0.848	42.45
2 mm	Top Right	1.895	1.972	3.90
	Middle Right	1.377	1.711	19.52
	Bottom Right	0.496	1.304	61.96
	Top Left	2.059	2.041	0.88
	Middle Left	1.576	1.700	7.29
	Bottom Left	0.628	1.086	42.17
2.5 mm	Top Right	2.367	2.483	4.67
	Middle Right	1.713	2.250	23.86
	Bottom Right	0.605	1.788	66.16
	Top Left	2.570	2.540	1.18
	Middle Left	2.001	2.260	11.46
	Bottom Left	0.764	1.674	54.36

Table 3. Average relative difference (ARD) for deformation measurement points.

Measured Point	Average ARD (%)	Max ARD (%)	Min ARD (%)
Top Right	3.5	4.67	1.42
Top Left	0.66	1.45	0.61
Middle Right	22.3	28.45	18.07
Middle Left	12.69	26.85	1.81
Bottom Right	58.91	66.16	50.90
Bottom Left	49.17	59.81	42.17

The force-displacement curve for experimental and numerical analyses was obtained from the compression test, as shown in Figure 6. After examining the three experimental studies, it was observed that yielding began around a force of 5750 N and a deformation of 1.4 mm. Numerical simulations exclusively simulated the elastic region, demonstrating elastic deformation up to 2.5 mm. Upon comparing the elastic portions, it is evident that the elastic curves have similar slopes, yet the limits of the elastic region are different. The yielding observed at around 1.4 mm deformation in the experimental studies is likely due to the disadvantages associated with FDM printers [40-42]. In the FDM process, porosity occurs in the material due to the inability to control thermal variation and humidity content [43, 44]. Among these disadvantages, the most significant reason is the decrease in the material's density and consequently its strength due to porosity [45].

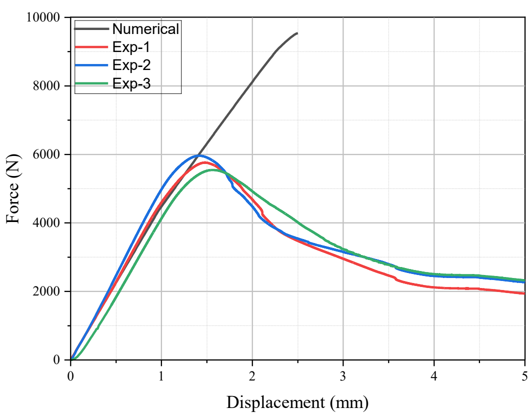

Figure 6. Experimental and numerical force-displacement curves for the BCCZZ lattice structure.

In the final step of the study, the results of experimental, numerical, and machine learning algorithms were comparatively analyzed in the elastic deformation region. Thus, it was determined which approach, the machine learning-based algorithm or the numerical model, aligns more closely with the experimental data. The MLR algorithm was trained using data obtained from compression test analyses conducted in Experiment 1 (Exp-1). Figure 7(a) presents a comparative analysis of the force values up to 1.5 mm deformation from experimental, numerical analyses and the MLR algorithm. In the MLR algorithm, the values of R^2, RMSE (Root Mean Square Error), MAE (Mean Absolute Error), and MAPE (Mean Absolute Percentage Error) are 0.97, 185.63, 158.25, and 4.38, respectively. Upon examining Figure 7(a), it was observed that the experimental and numerical data coincide regarding elastic deformation, while the MLR algorithm exhibited poorer performance compared to the numerical data. When analyzing the force-deformation graph, the experimental and numerical data almost align up to 0.6 mm, whereas the MLR algorithm has made a more distant prediction. The MLR algorithm, which constructs a linear regression line based on the training data, failed to accurately identify these points. Beyond 1.4 mm, as yielding began in the experimental data, neither the numerical analysis nor the MLR algorithm could predict the plastic deformation. This is because experimental data exhibit logarithmic variations, which the MLR algorithm inherently fails to capture due to its linear nature. To address this limitation, advanced algorithms such as polynomial regression, decision trees, or gradient boosting methods could be employed for better accuracy in modeling logarithmic changes.

The prediction error distribution of the MLR algorithm, depicted in Figure 7(b), reveals that the majority of errors cluster between -100 and 200, implying that most predictions closely approximate the actual values. However, due to the peaks in the 100-200 range, the errors deviate from a Gaussian normal distribution, indicating predictions further from the actual values. Therefore, the MLR algorithm has been less successful in the elastic region than the numerical method.

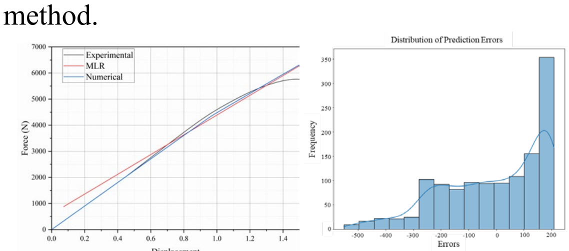

a) b)

Figure 7. a) Comparison of experimental, numerical, and MLR results in the elastic deformation region, b) Error distribution graph of the MLR algorithm.

4.CONCLUSIONS

In this study, the compression behavior of the BCCZZ lattice structure produced with eSUN PLA+ has been investigated through experimental, numerical, and MLR algorithms. The experimental analysis was compared with DIC analysis and numerical results. Additionally, the numerical results were compared with a machine learning algorithm developed using data obtained from the experimental study. The findings from the study are presented as follows:

● The error rates for the direction-dependent (-Y) deformation values measured at the top-right, top-left, middle-right, and middle-left points of the BCCZZ lattice structure subjected to the compression test were calculated to be 3.5%, 0.66%, 22.3%, and 12.69%, respectively. The measurements performed at these points have similar values when comparing DIC and numerical results.

● The error rates obtained at the bottom-right and bottom-left points were calculated as 58.91% and 49.17%, respectively. This is due to the specimen undergoing plastic deformation and failure at the bottom-right and bottom-left points under the applied force during the experiment measured with DIC. Since only elastic deformation is numerically modeled, high error rates have been observed at the lower points located on the base.

● The compression test results for elastic region deformation have been compared using experimental, numerical, and MLR algorithm analyses. Despite the MLR algorithm's R^2 value of 0.97, the numerical results correspond more closely with the experimental data in the elastic region deformation.

● Although the experimental findings align with the numerical and machine learning algorithms in the elastic region, this agreement does not extend to the plastic region. The early onset of plastic deformation in the experimental study compared to the numerical analysis is attributed to section narrowing and the tendency for easy separation between layers, which are drawbacks associated with FDM technology.

REFERENCES

1. Hirschberg, C., Larsen, M.S., Bøtker, J.P.,Rantanen, J., "Additive manufacturing of prototype elements with process interfaces for continuously operating manufacturing lines", Asian journal of pharmaceutical sciences, Vol. 13, Issue 6, Pages 575-583, 2018.

2. Ngo, T.D., Kashani, A., Imbalzano, G., Nguyen, K.T.,Hui, D., "Additive manufacturing (3D printing): A review of materials, methods, applications and challenges", Composites Part B: Engineering, Vol. 143, Pages 172-196, 2018.

3. Wang, Y., Zhou, Y., Lin, L., Corker, J.,Fan, M., "Overview of 3D additive manufacturing (AM) and corresponding AM composites", Composites Part A: Applied Science and Manufacturing, Vol. 139, Pages 106114, 2020.

4. Hanzl, P., Zetek, M., Bakša, T.,Kroupa, T., "The influence of processing parameters on the mechanical properties of SLM parts", Procedia Engineering, Vol. 100, Pages 1405-1413, 2015.

5. Ning, F., Cong, W., Qiu, J., Wei, J.,Wang, S., "Additive manufacturing of carbon fiber reinforced thermoplastic composites using fused deposition modeling", Composites Part B: Engineering. Vol. 80, Pages 369-378, 2015.

6. Seabra, M., Azevedo, J., Araújo, A., Reis, L., Pinto, E., Alves, N., Santos, R.,Mortágua, J.P., "Selective laser melting (SLM) and topology optimization for lighter aerospace componentes", Procedia Structural Integrity, Vol. 1, Pages 289-296, 2016.

7. Yuan, L., Ding, S.,Wen, C., "Additive manufacturing technology for porous metal implant applications and triple minimal surface structures: A review", Bioactive materials, Vol. 4, Pages 56-70, 2019.

8. Karayel, E.,Bozkurt, Y., "Additive manufacturing method and different welding applications", Journal of Materials Research and Technology, Vol. 9, Issue 5, Pages 11424-11438, 2020.

9. Delic, M.,Eyers, D.R., "The effect of additive manufacturing adoption on supply chain flexibility and performance: An empirical analysis from the automotive industry", International Journal of Production Economics, Vol. 228, Pages 107689, 2020.

10. Tang, C., Liu, J., Yang, Y., Liu, Y., Jiang, S.,Hao, W., "Effect of process parameters on mechanical properties of 3D printed PLA lattice structures", Composites Part C: Open Access. Vol. 3, Pages 100076, 2020.

11. Luo, J., Luo, Q., Zhang, G., Li, Q.,Sun, G., "On strain rate and temperature dependent mechanical properties and constitutive models for additively manufactured polylactic acid (PLA) materials", Thin-Walled Structures. Vol. 179, Pages 109624, 2022.

12. Samykano, M., "Mechanical property and prediction model for FDM-3D printed polylactic acid (PLA)", Arabian Journal for Science and Engineering, Vol. 46, Pages 7875-7892, 2021.

13. Singhvi, M., Zinjarde, S.,Gokhale, D., "Polylactic acid: Synthesis and biomedical applications", Journal of applied microbiology. Vol. 127, Issue 6, Pages 1612-1626, 2019.

14. Sharma, D.,Hiremath, S.S., "Experimental and FEM study on the in-plane and out-plane loaded reversible dual-material bio-inspired lattice structures with improved energy absorption performance", Composite Structures, Vol. 303, Pages 116353, 2023.

15. Takaichi, A., Kajima, Y., Kittikundecha, N., Htat, H.L., Cho, H.H.W., Hanawa, T., Yoneyama, T.,Wakabayashi, N., "Effect of heat treatment on the anisotropic microstructural and mechanical properties of Co–Cr–Mo alloys produced by selective laser melting", Journal of the Mechanical Behavior of Biomedical Materials, Vol. 102, Pages 103496, 2020.

16. Babamiri, B.B., Barnes, B., Soltani-Tehrani, A., Shamsaei, N.,Hazeli, K., "Designing additively manufactured lattice structures based on deformation mechanisms", Additive Manufacturing, Vol. 46, Pages 102143, 2021.

17. Maconachie, T., Leary, M., Lozanovski, B., Zhang, X., Qian, M., Faruque, O.,Brandt, M., "SLM lattice structures: Properties, performance, applications and challenges", Materials & Design, Vol. 183, Pages 108137, 2019.

18. Wu, W., Xia, R., Qian, G., Liu, Z., Razavi, N., Berto, F.,Gao, H., "Mechanostructures: Rational mechanical design, fabrication, performance evaluation, and industrial application of advanced structures", Progress in Materials Science, Vol. 131, Pages 101021, 2023.

19. Köhnen, P., Haase, C., Bültmann, J., Ziegler, S., Schleifenbaum, J.H.,Bleck, W., "Mechanical properties and deformation behavior of additively manufactured lattice structures of stainless steel", Materials & Design, Vol. 145, Pages 205-217, 2018.

20. Mines, R., Tsopanos, S., Shen, Y., Hasan, R.,McKown, S., "Drop weight impact behaviour of sandwich panels with metallic micro lattice cores", International Journal of Impact Engineering, Vol. 60, Pages 120-132, 2013.

21. Wang, W., Wang, T.Y., Yang, Z., Liu, L., Tong, X., Tong, W., Deng, J., Chen, F.,Liu, X., "Cost-effective printing of 3D objects with skin-frame structures", ACM Transactions on Graphics (ToG), Vol. 32, Issue 6, Pages 1-10, 2013.

22. Zhou, X., Qu, C., Luo, Y., Heise, R.,Bao, G., "Compression behavior and impact energy absorption characteristics of 3D printed polymer lattices and their hybrid sandwich structures", Journal of Materials Engineering and Performance, Vol. 30, Pages 8763-8770, 2021.

23. Seremet, H.,Babacan, N., "Compressive properties of AlSi10Mg lattice structures with novel BCCZZ and FCCZZ configurations fabricated by selective laser melting", Rapid Prototyping Journal, Vol. 30, Issue 4, Pages 770-781, 2024.

24. Ramos, H., Pickering, E., AlMahri, S., Krishnan, K., Oyebanji, J., Guan, Z., Langdon, G.,Santiago, R., "Experimental evaluation of hybrid lattice structures subjected to blast loading". Additive Manufacturing. Vol. 76, Pages 103751, 2023.

25. Araghi, M., Rokhgireh, H.,Nayebi, A., "Experimental and FEM investigation of BCC lattice structure under compression test by using continuum damage mechanics with micro-defect closure effect". Materials & Design. Vol. 232, Pages 112125, 2023.

26. Gonabadi, H., Yadav, A.,Bull, S., "The effect of processing parameters on the mechanical characteristics of PLA produced by a 3D FFF printer", The International Journal of Advanced Manufacturing Technology, Vol. 111, Pages 695-709, 2020.

27. Song, J., Wang, Y., Zhou, W., Fan, R., Yu, B., Lu, Y.,Li, L., "Topology optimization-guided lattice composites and their mechanical characterizations", Composites Part B: Engineering, Vol. 160, Pages 402-411, 2019.

28. Drücker, S., Lüdeker, J.K., Blecken, M., Kurt, A., Betz, K., Kriegesmann, B.,Fiedler, B., "Probabilistic analysis of additively manufactured polymer lattice structures", Materials & Design, Vol. 213, Pages 110300, 2022.

29. Kolken, H., Garcia, A.F., Du Plessis, A., Meynen, A., Rans, C., Scheys, L., Mirzaali, M.,Zadpoor, A., "Mechanisms of fatigue crack initiation and propagation in auxetic meta-biomaterials", Acta biomaterialia, Vol. 138, Pages 398-409, 2022.

30. Hedayati, R., Sadighi, M., Mohammadi-Aghdam, M.,Zadpoor, A., "Analytical relationships for the mechanical properties of additively manufactured porous biomaterials based on octahedral unit cells", Applied Mathematical Modelling, Vol. 46, Pages 408-422, 2017.

31. Yavas, D., Liu, Q., Zhang, Z.,Wu, D., "Design and fabrication of architected multi-material lattices with tunable stiffness, strength, and energy absorption", Materials & Design, Vol. 217, Pages 110613, 2022.

32. Liu, C., Lertthanasarn, J.,Pham, M.-S., "The origin of the boundary strengthening in polycrystal-inspired architected materials". Nature Communications, Vol. 12, Issue 1, Pages 4600, 2021.

33. Mostafa, K.G., Momesso, G.A., Li, X., Nobes, D.S.,Qureshi, A.J., "Dual graded lattice structures: generation framework and mechanical properties characterization", Polymers, Vol. 13, Issue 9, Pages 1528, 2021.

34. Saleh, M., Anwar, S., Al-Ahmari, A.M.,Alfaify, A., "Compression performance and failure analysis of 3D-printed carbon fiber/PLA composite TPMS lattice structures", Polymers, Vol. 14, Issue 21, Pages 4595, 2022.

35. *eSUN PLA+ filament,* https://www.esun3d.com/pla-pro-product/, May 5, 2024.

36. Hauswirth, S.M., Bierkens, M.F., Beijk, V.,Wanders, N., "The potential of data driven approaches for quantifying hydrological extremes", Advances in Water Resources, Vol. 155, Pages 104017, 2021.

37. Zhao, X., Zhang, R., Chen, F., Maisupova, B., Kirillov, V., Mambetov, B., Yu, S., He, Q., Dosmanbetov, D.,Kelgenbayev, N., "Reconstructed summertime (June–July) streamflow dating back to 1788 CE in the Kazakh Uplands as inferred from tree rings", Journal of Hydrology: Regional Studies, Vol. 40, Pages 101007, 2022.

38. Ren, X., Mi, Z.,Georgopoulos, P.G., "Comparison of Machine Learning and Land Use Regression for fine scale spatiotemporal estimation of ambient air pollution: Modeling ozone concentrations across the contiguous United States". Environment international, Vol. 142, Pages 105827, 2020.

39. Xie, X., Wu, T., Zhu, M., Jiang, G., Xu, Y., Wang, X.,Pu, L., "Comparison of random forest and multiple linear regression models for estimation of soil extracellular enzyme activities in agricultural reclaimed coastal saline land", Ecological Indicators, Vol. 120, Pages 106925, 2021.

40. Baechle-Clayton, M., Loos, E., Taheri, M.,Taheri, H., "Failures and flaws in fused deposition modeling (FDM) additively manufactured polymers and composites", Journal of Composites Science, Vol. 6, Issue 7, Pages 202, 2022.

41. Moradi, M., Karami Moghadam, M., Shamsborhan, M.,Bodaghi, M., "The synergic effects of FDM 3D printing parameters on mechanical behaviors of bronze poly lactic acid composites", Journal of Composites Science, Vol. 4, Issue 1, Pages 17, 2020.

42. Khosravani, M.R., Božić, Ž., Zolfagharian, A.,Reinicke, T., "Failure analysis of 3D-printed PLA components: Impact of manufacturing defects and thermal ageing", Engineering Failure Analysis, Vol. 136, Pages 106214, 2022.

43. Bhagia, S., Bornani, K., Agrawal, R., Satlewal, A., Ďurkovič, J., Lagaňa, R., Bhagia, M., Yoo, C.G., Zhao, X.,Kunc, V., "Critical review of FDM 3D printing of PLA biocomposites filled with biomass resources, characterization, biodegradability, upcycling and opportunities for biorefineries", Applied Materials Today, Vol. 24, Pages 101078, 2021.

44. Swetham, T., Reddy, K.M.M., Huggi, A.,Kumar, M.N., "A Critical Review on of 3D Printing Materials and Details of Materials used in FDM", Int. J. Sci. Res. Sci. Eng. Technol., Vol. 3, Issue 2, Pages 353-361, 2017.

45. Triyono, J., Sukanto, H., Saputra, R.M.,Smaradhana, D.F., "The effect of nozzle hole diameter of 3D printing on porosity and tensile strength parts using polylactic acid material", Open Engineering. Vol. 10, Issue 1, Pages 762-768, 2020.